IECO International Journal Of Industrial Electronics Control and Optimization
Print ISSN: 3517-2645
Online ISSN: 3568-2645
Homepage: https://ieco.usb.ac.ir/

Robust Beamforming for Ultrasonic Imaging using Wavelet-based Thresholding and Coherence Weighting

Mozhgan Ehsani[1] | Mehdi Bekrani[2] | Solyman Garousi[3]

Department of Electrical and Computer Engineering, Qom University of Technology (QUT), Qom, Iran [1,2,3]
Corresponding author's email: bekrani@qut.ac.ir

Article Info

Article type:
Research Article

Article history:
Received: 05-May-2024
Received in revised form: 05-Aug-2024
Accepted: 12-Aug-2024
Published online: 21-Dec-2024

Keywords:
Coherence weighting,
Covariance matrix,
Delay-and-sum beamformer,
MV beamformer,
Ultrasonic waves.

ABSTRACT

The delay-and-sum (DS) beamforming and delay-weight-and-sum (DWS) beamforming are primary methods in ultrasonic imaging with phased arrays. Total focusing method (TFM) and Minimum Variance (MV) based adaptive beamforming are well-known methods within DS and DWS beamforming, respectively. The MV-based adaptive beamforming significantly reduces interferences and provides high-resolution image compared to TFM beamforming, at the cost of high computational complexity, and sensitivity to input statistics for matrix inversion. To address these challenges, recently, iterative MV (IMV) has been proposed to alleviate computational burdens without the need for matrix inversion. The delay-multiply-and-sum (DMAS) beamforming enhances TFM beamforming performance by employing spatial information of the array signals. However, the resulting images remain susceptible to speckle and background noises in all of these beamformers. In this paper, we aim to improve these beamforming methods so that speckle and Gaussian background noise are reduced while preserving the quality of the reflective echoes in ultrasonic images. In the proposed method, a wavelet transform with a novel threshold function is applied to the received signals to initially reduce the noise, followed by the application of the beamformer. Subsequently, the coherence weighting using the denoised signals is derived, and the obtained coherence weighting is then integrated into the beamforming process. Simulation results demonstrate that the proposed method achieves a significant reduction in background noise and speckles of the above beamformer, and particularly reduces background noise and speckles of beamformer up to approximately -27dB while preserving the detection capability of reflective points.

I. Introduction

Today, ultrasound imaging systems commonly utilize Delay-and-Sum (DS) beamformers. These types of beamformers operate in a fast and simple manner but provide images with low resolution [1]. Synthetic Aperture Focusing Technique (SAFT) and Total Focusing Method (TFM) are two widely used DS based imaging methods[2-4].

One of the advanced beamforming methods in ultrasonic imaging with phased array is the Delay-Weight-and-Sum (DWS) beamforming, which operates by weighting the delayed signals and then summing them. The adaptive beamforming method based on the Minimum Variance (MV) theory is a well-known beamforming method within the context of DWS beamforming techniques.

In the MV adaptive beamformer, high-resolution and high-contrast images are generated. The associated weights are determined at each moment in such a way that the output power of the beamformer reaches the minimum possible value while preserving the desired signal.

The MV adaptive beamforming method involves a significant computational complexity. In recent years, approaches have been proposed to reduce the computational complexity of the MV beamforming technique[1]. In the Decimated MV (DMV) method, which prioritizes focusing during the ultrasonic wave transmission phase, a uniform reduction of array information is achieved by applying a spatial low-pass frequency filter. This reduction doesn't compromise the effective signal information contained within the reduced array covariance matrix[5]. Another approach to low-complexity MV beamforming involves transferring data to the beam space. This has been proposed utilizing various transformations such as the Discrete Fourier Transform (DFT), Discrete Cosine Transform (DCT), or Legendre Polynomial Transform[6]. The iterative MV (IMV) based adaptive beamforming method exploits the fact that received signals from two adjacent imaging points in ultrasonic imaging do not differ significantly. A new formula for updating the weights is presented, which eliminates the need for computing the covariance matrix inverse and results in faster optimization with just a few iterations for each imaging point [7].

In[8, 9], low-complexity and robust MV beamformers are proposed for ultrasound imaging systems using beamspace dominant mode rejection (DMR). In DMR technique, only eigenvectors corresponding to a few largest eigenvalues are computed. Computational complexity is reduced by predicting element-space data to the beam space domain and then employing dominant mode removal on the beam-space covariance matrix.

The Adaptive Spatial Smoothing MV (ASS-MV) method enhances the resolution and the ratio of contrast enhancement to noise of the MV method, by specifying subarray lengths for spatial smoothing, while preserving MV performance [10]. Moreover, the Generalized Sidelobe Canceller (CSG) partially suppresses MV method by dividing the weight vector into two parts in an adaptive manner [11]. Additionally, a Fast Adaptive Beamforming with sidelobe control is proposed, which minimizes the sidelobe level [12].

Recent advancements in ultrasonic imaging for non-destructive testing (NDT) have introduced innovative approaches to enhance defect detection and image quality. In[13], a full-matrix imaging method based on the search-vector imaging condition is proposed to detect the defects. The search-vector imaging condition integrates waveform inversion using first-order derivative vectors and approximated Hessian matrices to achieve highly accurate defect detection in complex-surface components.

Ref. [14] proposes a cost-effective imaging method utilizing Full Matrix Migration Total Focus Method (FM-TFM) and normalized cross-correlation (NCC) template matching, offering large-area scanned images without costly equipment.

In[15], a discretized tensor-based model for TFM, employing a sparse regularization strategy significantly enhances defect characterization and noise suppression, outperforming traditional TFM in both simulation and experimental studies. In[16], an optimized TFM based on delay-multiply-and-sum (DMAS) beamforming improves imaging performance through synthetic focusing in TFM, promising enhanced accuracy and quality in NDT applications.

Some recent studies in the field of NDT have focused on leveraging artificial neural networks, particularly deep learning techniques, to enhance inspection processes. In [17], a conditional Generative Adversarial Network (cGAN) was employed to replace conventional Full Matrix Capture (FMC) and Total Focusing Method (TFM) procedures with a simplified zero-degree plane wave. This approach demonstrated comparable resolution to TFM while significantly improving contrast in over 94% of reconstructions.

Reference [18] introduced a deep neural network (DNN) tailored for ultrasonic array tomography, specifically targeting subsurface crack recognition and pixel-wise cross-section image reconstruction in reinforced concrete structures. The DNN adopted an encoder-decoder architecture enhanced by skip connections and residual modules, effectively adapting to the semantic structure of ultrasonic B-scans. In[19], researchers developed a deep-learning surrogate model for rapid generation of realistic ultrasonic images in the Multi-modal Total Focusing Method (M-TFM). Using a Conditional U-Net (cU-Net), they facilitated controlled generation of high-resolution M-TFM images. This approach was validated with a case study involving planar defects in a complex weld-like profile, addressing uncertainties in image parameter reconstruction through numerical and experimental data.

While various beamforming methods aim to generate the ultrasonic image with high resolution and low complexity, they are sensitive to noises and may fail to detect the reflectors in noisy situations.

On the other hand, using deep learning in NDT offers significant benefits but also faces challenges. Deep learning models require large, labeled datasets for effective training, which can be costly and time-consuming to obtain, especially for diverse or rare defects. Additionally, their computational demands and concerns about robustness in noisy environments pose further obstacles.

In this paper, we propose a noise robust beamforming method to enhance the TFM, DMAS, MV, and IMV methods in a way that reduces background speckle and Gaussian noises in the resulting images. To achieve this, we employ a coherence weighting method [3] along with thresholding in the wavelet transform [20] to remove noise from ultrasonic images. An improved thresholding function, based on logistic function, is introduced to denoise images generated by the mentioned beamformers.

The remainder of this paper is organized as follows. In Section II, some well-known beamformers are introduced. In Section III, we propose a new noise robust beamforming method for ultrasonic imaging. The simulation and experimental results are conducted in Section IV. Conclusion is finally given in Section V.

II. Beamforming methods

In this section, we outline several beamforming methods. Our objective is to enhance their performance and make them more robust to noise using the proposed denoising method.

A. Delay-and-Sum (DS) beamformer

In the DS beamformer, suitable delays are initially applied to the received signals of the array elements to compensate for path delays. Subsequently, these signals are summed with constant weighting coefficients. If $z_j[n]$ represents the measured signal of element j at time index n, then

$$x_j[n] = z_j\left[n - \Delta_j[n]\right] \tag{1}$$

where $\Delta_j[n]$ represents the delay of element j relative to time index n, and $x_j[n]$ is the delayed signal received by element j .

To obtain the output of the DS beamformer, a constant weight is used, represented by:

$$y_{DAS}[n] = \sum\nolimits_{j=1}^{M} w_j^* x_j[n] = \boldsymbol{w}^H \boldsymbol{x}[n] \tag{2}$$

where $*$ denotes the conjugate transpose, H denotes the Hermitian transpose, and w_j^* is the weight applied to element j in the DS beamformer, which is obtained as a constant vector from [21, 22]:

$$w_{DS}(n) = \frac{1}{M}\vec{1} \tag{3}$$

where M is the number of array elements. In (2), we define vector $\mathbf{x}[n]$ as $\boldsymbol{x}[n] = \left[x_1[n], x_2[n], \dots, x_M[n]\right]^T$ and $\boldsymbol{w} = [w_1^*, w_2^*, \dots, w_M^*]^T$.

In the SAFT method, each array element transmits a signal and receives the signal reflection from the same element. Therefore, the brightness intensity of each pixel in the image is calculated as follows [22]

$$I_{SAFT}(n) = \sum_{i=1}^{M} A_i(x_{si}, 2\tau_i) \tag{4}$$

where x_{si} is the longitudinal coordinate (the length) of the ith element, $A_i(.)$ is the pulse-echo response of the ith element, and τ_i is the time it takes for the signal to travel from the ith element to the point of interest, which is the location of a specified pixel in the ultrasonic image.

In the TFM method, each array element individually transmits a signal, and the signal reflection is received by all array elements [22]. As a result, the brightness intensity of each pixel in the image is calculated as follows:

$$I_{TFM}(n) = \sum_{i=1}^{M}\sum_{j=1}^{M} A_{i,j}\left(x_{si}, x_{rj}, \tau_i + \tau_j\right) \tag{5}$$

where x_{si} and x_{rj} are the longitudinal coordinates of the transmitting and receiving elements, respectively, $A_{i,j}(.)$ is the pulse-echo response received by the jth element and transmitted by the ith element, and τ_i and τ_j are the times traveled from the transmitting element i to the point of interest and from the point of interest to the receiving element j, respectively.

B. Delay-Multiply-and-Sum (DMAS) beamformer

In[16], an optimized total focusing method using the delay-multiply-and-sum (DMAS) approach was proposed. For a given point z in the imaging area, the focused signal relative to z in DMAS is described as follows:

$$I_{DMAS}(z) = \sum_{i=1}^{M-1}\sum_{j=i+1}^{M} sign\left\{S_i(z)S_j(z)\right\}\sqrt{\left|S_i(z)S_j(z)\right|} \tag{6}$$

Here, the sign function denotes the signum function extraction operation, and the signed square root calculation ensures that the amplitude of each multiplication term is correctly scaled to match the dimensionality of the echo signals. S_j is the result of all echo signals received by the j-th element, calculated as:

$$S_j(z) = \sum_{k=1}^{M} A_{k,j}\left(x_{sk}, x_{rj}, \tau_k + \tau_j\right) \tag{7}$$

where, similar to TFM, τ_k and τ_j are the travel times from the transmitting element k to the point of interest and from the point of interest to the receiving element j, respectively.

C. MV beamformer

The MV beamformer updates the weight vector for each point in the image based on the received data, adjusting the weights in such a way that the maximum level of interference and noise is removed from the desired signal. The output of this beamformer is obtained from:

$$y_{MV}[n] = \sum\nolimits_{j=1}^{M} w_{jMV}^* x_j[n] = \boldsymbol{w}_{MV}^H \boldsymbol{x}[n] \tag{8}$$

where x_j is the delayed signal received by element j, and w_{jMV}^* is the weight applied to element j in the MV beamformer. This beamformer minimizes the output power while preserving the desired signal unchanged, as described by:

$$\min_{w_{MV}}\{w_{MV}^H[n]x[n]w_{MV}[n]\} \ subject\ to\ w_{MV}^H[n]a = 1 \tag{9}$$

where $\mathbf{a}$ is the steering vector towards the desired signal. Since $\mathbf{x}[n]$ has been previously delayed, $\mathbf{a}$ is a column vector of size $M \times 1$ consisting of unit values, i.e., $\mathbf{a} = [1,1,\dots,1]_M^T$. The objective is to find $\mathbf{w}[n]$ such that the expression $\mathbf{w}_{MV}^H[n]\mathbf{x}[n]\mathbf{w}_{MV}[n]$ is minimized and the value of the beamforming gain $\sum_j w_j[n]$ is equal to one. To this end, optimized weights are obtained using the following equation:

$$\boldsymbol{W}_{MV}[n] = \frac{\boldsymbol{R}^{-1}[n]\boldsymbol{a}}{\boldsymbol{a}^H\boldsymbol{R}^{-1}[n]\boldsymbol{a}} \tag{10}$$

where $\boldsymbol{R}[n]$ is the autocorrelation function of the output data of the phased array elements, obtained from:

$$\boldsymbol{R}[n] = E\{\boldsymbol{x}[n]\boldsymbol{x}^H[n]\} \tag{11}$$

in which $E\{.\}$ represents statistical averaging. To accelerate the algorithm in online implementation, instantaneous values of the vectors are used instead of averaging for calculating the autocorrelation function. Therefore, the instantaneous autocorrelation function is given by:

$$\boldsymbol{R}[n] \approx \boldsymbol{x}[n]\boldsymbol{x}^H[n] \tag{12}$$

The covariance matrix of the array is estimated from the measured signals using[23, 24]:

$$\boldsymbol{R}[n] = \sum_{j=1}^{M} x_j[n]x_j^H[n] + \delta\boldsymbol{I} \tag{13}$$

where the regularization term $\delta\boldsymbol{I}$ is used to increase numerical stability and robustness of the MV method, in which $\boldsymbol{I}$ is the identity matrix and δ is a small positive constant close to zero.

D. IMV beamformer

To reduce the computational complexity of the MV method while preserving its performance, and increase its robustness against correlation matrix inverse errors, the IMV beamformer has been proposed [7]. In this approach, weights are updated iteratively using the steepest descent method. Therefore, the final equation for obtaining the weight vector is as follows:

$$\begin{aligned}\boldsymbol{w}_{D+1}[n] = [\boldsymbol{I} - \boldsymbol{a}(\boldsymbol{a}^H\boldsymbol{a})^{-1}\boldsymbol{a}^H][\boldsymbol{I} - \mu\boldsymbol{R}]\boldsymbol{w}_D[n] \\ +\boldsymbol{a}(\boldsymbol{a}^H\boldsymbol{a})^{-1}\end{aligned} \tag{14}$$

where the index D indicates the number of repetitions, and μ represents the step size. Due to the fact that the received signal from one imaging point does not change significantly compared to the received signal from another nearby point, the initial weight ($\mathbf{w}_0[n]$) is adjusted based on the last weight vector found for the previous point (i.e., $\mathbf{w}_0[n] = \mathbf{w}[n-1]$). This approach accelerates convergence speed [7]. The step size μ is also set to the maximum available value, calculated as $\mu = \frac{2}{\mathrm{trace}(\mathbf{R})}$[25].

By using the termination criterion $||y_D[n]|^2 - |y_{D-1}[n]|^2|$, where $y_D[n]$ represents the output of the array in the Dth repetition, the changes in output power can be determined at each iteration. When this criterion is less than a predefined threshold through trial and error, the iteration is terminated [7].

III. The Proposed Method

In the proposed method, we aim to eliminate noise generated in ultrasonic imaging and obtain higher quality images by using wavelet transform and coherence weighting. Fig. 1 illustrates the overall block diagram of the proposed approach. As shown, after receiving signals from the ultrasonic phased array, appropriate delays are applied to the signals to focus the beam on a target point (which will form a pixel of the ultrasonic image). We then use the wavelet transform to remove noise from the delayed received signals. Specifically, the signals are decomposed using the wavelet, and then the noise is reduced or removed using the threshold function proposed in this paper.

Finally, the noise-free signal is reconstructed using the inverse wavelet transform on the modified coefficients. These denoised signals are then used to compute coherence weighting and beamforming for the target point. The calculated coherence coefficients are multiplied at the output of the beamformer, and the brightness intensity of the target pixel in the image is obtained. This process is repeated for all pixels in the image, and the information of each pixel is stored in a buffer to create the final image. In this proposed method, the resulting image not only reduces the background noise and speckles but also enhances the resolution and the ability to distinguish reflective points of the test piece from each other.

The steps of the proposed method are as follows:

I. Wavelet Packet Transform (WPT) is used to decompose the signal and a proposed thresholding method is applied to remove noise from the received signals.

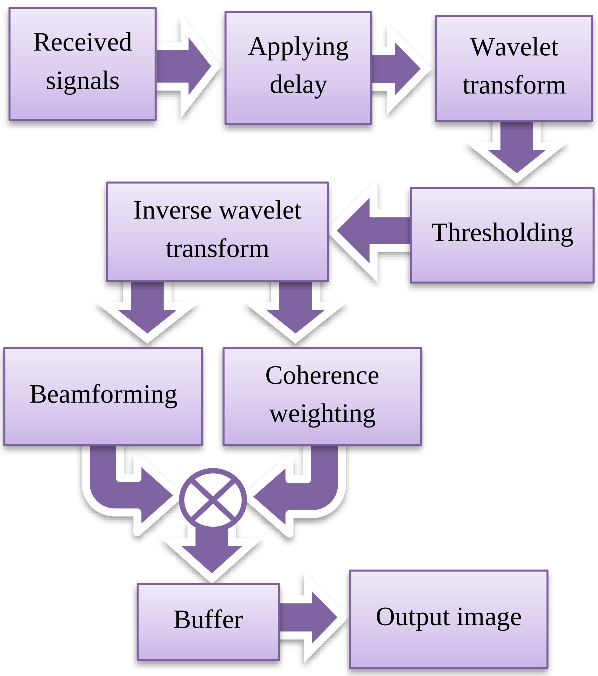

Fig. 1. Block diagram of the proposed method, illustrating the process from the received signals of the phased array to the output image construction.

II. Using the denoised signals and the optimization formula for weights in the TFM/MV/IMV methods, the ultrasound image of the under-test piece is obtained.

III. Using the denoised signals from the previous step, coherence weights are calculated for the image obtained by the beamformer.

IV. By applying the calculated coherence weights to the denoised beamformed image, an image with minimal noise is obtained.

The details of the wavelet transform and coherence weighting in the proposed method will be explained further.

A. *Wavelet Transform*

Removing Speckle and Gaussian noises using wavelet transform based on the fact that only a few wavelet coefficients contain the highest signal power, while the rest typically have low noise values, is feasible[26]. The wavelet transform performs noise reduction in three steps:

1) The signal is decomposed using various methods, one of which is the Wavelet Packet Transform (WPT). In this transform, the signal is divided into two parts: approximation and details, which respectively contain low-frequency and high-frequency information. The approximation part is successively decomposed into multiple stages with wavelet transform to obtain more details, and the details part is further divided into approximation and details at each level. This method provides high precision in signal reconstruction[27].

2) In this stage, the coefficients of the approximation and details parts are thresholded to remove coefficients that contain insignificant noise.

3) After thresholding the coefficients, the noise-reduced signal is reconstructed using the modified approximation and details coefficients through inverse wavelet transform.

The following effective threshold value for ultrasound signals has been applied as introduced in[28]:

$$T = \sqrt{\mu_j + k\sigma_j} \tag{15}$$

in which the parameter T represents the threshold value, μ_j denotes the mean value, and σ_j represents the standard deviation.

Two threshold functions, hard and soft, are commonly used for thresholding[29]. However, due to the issues these two thresholds create in signal reconstruction, we develop an alternative function to overcome the shortcomings of classical threshold functions. This alternative is based on the logistic function, which strikes a balance between the advantages and disadvantages of hard and soft thresholds.

The logistic function is a type of sigmoid function that is real-valued, bounded, and differentiable. It is defined for all real values, has a positive derivative for all its values, and is expressed by:

$$y = \frac{\alpha}{1 + e^{-\beta(x-\gamma)}} \tag{16}$$

in which, α represents the maximum value of the function, β determines the steepness of the curve, and γ specifies the center of the function. With the aid of this function, the improved threshold function is introduced. In this proposed improved threshold function, to ensure that coefficients' values are not zero for values smaller than the threshold level, the thresholding function is extended by incorporating the solution presented in[30]. This extension attenuates values between T and $-T$ instead of setting them to zero, as expressed by:

$$f(x) = \begin{cases} x - \left(\frac{T}{1+e^{-c(x-T)}}\right) & x > T \\ sgn(x)\left(\frac{|x|^d}{2T^{d-1}}\right) & |x| \le T \\ x + \left(\frac{T}{1+e^{-c(x+T)}}\right) & x < -T \end{cases} \tag{17}$$

where the parameter $c \geq 0$ controls the attenuation of values greater than the threshold level T and values smaller than $-T$, and the even parameter $d = 2k, k \in \mathbb{N}$ controls the attenuation of values between T and $-T$. In this threshold function, we have a better control over the impact of samples close to the threshold levels $\pm T$. If c and d tend to infinity, the threshold function behaves similarly to a hard threshold but remains continuous. This function possesses properties of continuity, uniformity, and differentiability over the entire domain interval $(-\infty, +\infty)$. The curves of the proposed function for $T = 3$ are shown in Fig. 2 for some values of c and d.

As shown in Fig. 2, when $c = 100$ and $d = 150$, the thresholding function behaves like a hard thresholding method. This means that wavelet coefficients within the range of (-3, +3) are set to zero, while those outside this range retain their values. Conversely, for smaller values of c and d, the function attenuates the magnitude of wavelet coefficients within the range of (-3, +3), with smaller coefficients being more heavily attenuated towards zero. For coefficients outside the range of (-3, +3), there is also attenuation, but the reduction in magnitude is less pronounced for larger coefficients. Specifically, when $c = 1$ and $d = 4$, the curves are smoothest, resulting in minimal attenuation for wavelet coefficients within the range of (-3, +3) and significant attenuation for those outside this range.

B. Coherence Weighting

The concept of coherence weighting was first introduced as the ratio between the coherence sum and the total addition of the signal magnitudes[31]. In order to minimize background noise and mitigate the effect of stray radiation in shaping different radiation patterns, coherence weighting can be employed. It is calculated according to the following equation[32]:

$$CF(s) = \left(\frac{|I(s)|^2}{M^2 \sum_{i=1}^{M} \sum_{j=1}^{M} \left| A_{i,j}\left(x_{si}, x_{rj}, \tau_i + \tau_j\right) \right|^2} \right)^{p_{cf}} \tag{18}$$

where $I(s)$ represents the intensity of each pixel in the image s, derived by the specified beamforming method, M is the number of elements in the array, x_{si} and x_{rj} represent the longitudinal coordinates of the transmitting and receiving elements, respectively. $A_{i,j}(.)$ signifies the pulse-echo response received by element j transmitted by element i, and τ_i and τ_j denote the time taken from the transmitting element i to the point of interest and from the point of interest to the receiving element j, respectively.

Additionally, p_{cf} (phase coherence factor) is the sensitivity factor, which governs the relationship between regions with different levels of coherence.

Multiplying the value of coherence weighting by the output images of the different beamformers results in their noise-removed images according to:

$$I_{CF}(x, y) = CF(x, y) I(x, y) \tag{19}$$

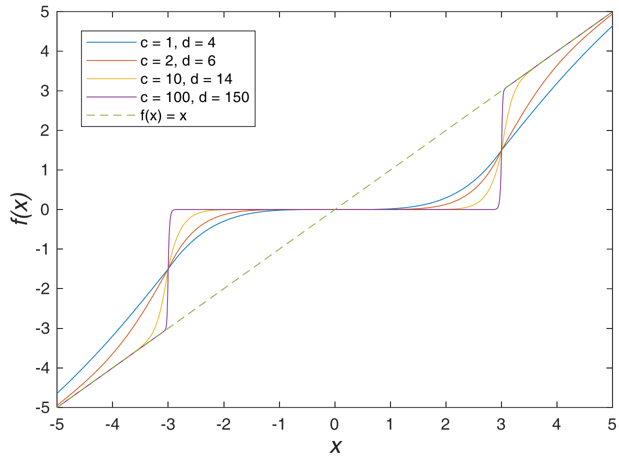

Fig. 2. The curves of the proposed thresholding function for various values of c and d.

where $CF(x, y)$ represents the coherence weighting, $I(x, y)$ denotes the image obtained from different beamformers, and $I_{CF}(x, y)$ is the denoised image.

In the proposed method, the WPT is utilized to decompose the signal using the effective threshold presented in (15) and the proposed threshold function using (17) to eliminate noise from the received signals. The signal decomposition levels are set to two, and the Daubechies wavelet of type 4 (db4) is employed for the ultrasonic signal. The beamformer weights are subsequently derived using (3), (10), and (14) for TFM, MV, and IMV, respectively, and the denoised image is generated. Using the denoised signals obtained in the previous stage and (18), the coherence weights are calculated. By applying the calculated weights to the denoised image generated by the specified beamformer, using (19), an image with minimal noise is obtained.

IV. Simulation and Experimental Results

The proposed method has been evaluated using simulation and experiments.

A. Simulation results

Simulation is conducted using MATLAB software. In the simulation, a steel specimen with dimensions of 75mm×50mm containing four point-defects, as depicted in Fig. 3, was tested. It is assumed in the simulations that there is no distance between the phased array and the steel specimen. Speckle noise with SNR=4 dB and Gaussian white noise with SNR=0dB have been added to the ultrasonic signals. To generate the speckle noise, we add some correlated extra peaks to the received signals of the phased array. These extra peaks are similar to the peaks of the actual reflections from defects. The simulation setup parameters are summarized in Table 1.

In our simulations, the values of c, d, and p_{cf} are determined empirically to achieve effective noise reduction from received ultrasonic phased array signals. The values of

TABLE 1 PARAMETERS OF SIMULATION SETUP

Material	Steel
Piece height (mm)	25
Number of array elements	16
Element pitch (mm)	2
Received signal type	5 cycles of modulated sinusoidal waveform
Probe frequency (MHz)	5
Sampling rate (MHz)	40
Speed of sound in steel (m/s)	3000
Image resolution (mm)	0.5
p_{cf}	4
c	5
d	30

other parameters are typically chosen to simulate realistic conditions.

To evaluate the performance of the beamformer, we utilize the following metrics:

1) Array Performance Index (API)

API is a dimensionless metric used to quantitatively compare the performance of array inspection methods in terms of their capability to detect and image reflector points[33]. A lower value of this index indicates better noise removal performance. API is computed giving:

$$API = \frac{A_{-6dB}}{\lambda^2} \tag{20}$$

where A_{-6dB} represents the area of the region where the value is at most, 6dB less than the maximum point, and λ denotes the wavelength of the ultrasonic signal.

2) Average Background Noise

Average noise (N_{avg}) is the mean intensity level of the pixels in the image corresponding to non-reflective points.

As N_{avg} decreases, the background brightness of the image decreases, leading to more accurate detection of reflective points.

3) Intensity Function

The intensity function is expressed as the normalized maximum intensity within the image depth range, obtained for each length x according to the following equation:

$$F(x) = 10\, log_{10} \left\{ f(x) / \max_{x} f(x) \right\} \tag{21}$$

where the function $f(x)$ provides the maximum intensity level for each specified length x, thus $f(x) = \max_{z}\{I(x,y)\}$.

Based on the function $F(x)$, the separability of reflective points in the image from each other, the maximum attenuation level of the image for reflective points, and the average background noise level in the image are assessed [24].

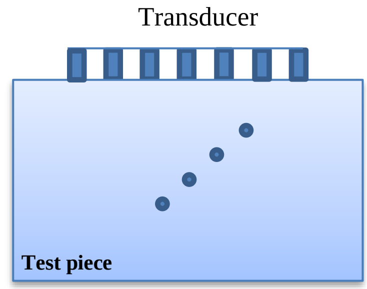

Fig. 3. The steel piece under test with four point-defects. The transducer, an ultrasonic phased array, is mounted directly over the piece.

Fig. 4 illustrates simulated images of TFM, DMAS, MV, and IMV beamforming methods without denoising (first column), with coherence weighting alone (second column), and the denoised images using the proposed wavelet thresholding along with coherence weighting (third column).

As observed in Fig. 4, applying coherence weighting alone to the beamforming methods has effectively increased image clarity to the extent that reflective points become more distinguishable from background noises. However, the amount of background noises is still high, which affect the image quality. As can be seen, the proposed method further enhances the image quality with lowering the background noises. Therefore, this approach exhibits a high capability in reflective point detection and background noise elimination. Particularly, in the IMV beamforming, it is clear through Fig. 4 that while coherence weighting alone reduces image noise substantially, our proposed denoising method enhances defect detection by producing brighter reflective points and lower background noise.

Fig. 5 depicts the intensity function for the TFM, MV, IMV, and DMAS methods in the noisy condition using (21). As evident in Fig. 5, in the presence of noise, IMV and DMAS methods present reflective points with higher discrimination compared to the other two methods. Additionally, Fig. 6 illustrates the intensity plots for the TFM, MV, IMV, and DMAS methods with the application of coherence weighting alone.

Comparing Fig. 6 with Fig. 5 demonstrates the positive impact of coherence weighting on the clarity of reflective points, the distinguishability of these points from each other, and significant background noise reduction. It is also noticeable that applying this weighting to these methods has led to the creation of more discriminated peaks in the intensity plot, indicating an enhanced ability to detect the reflective points.

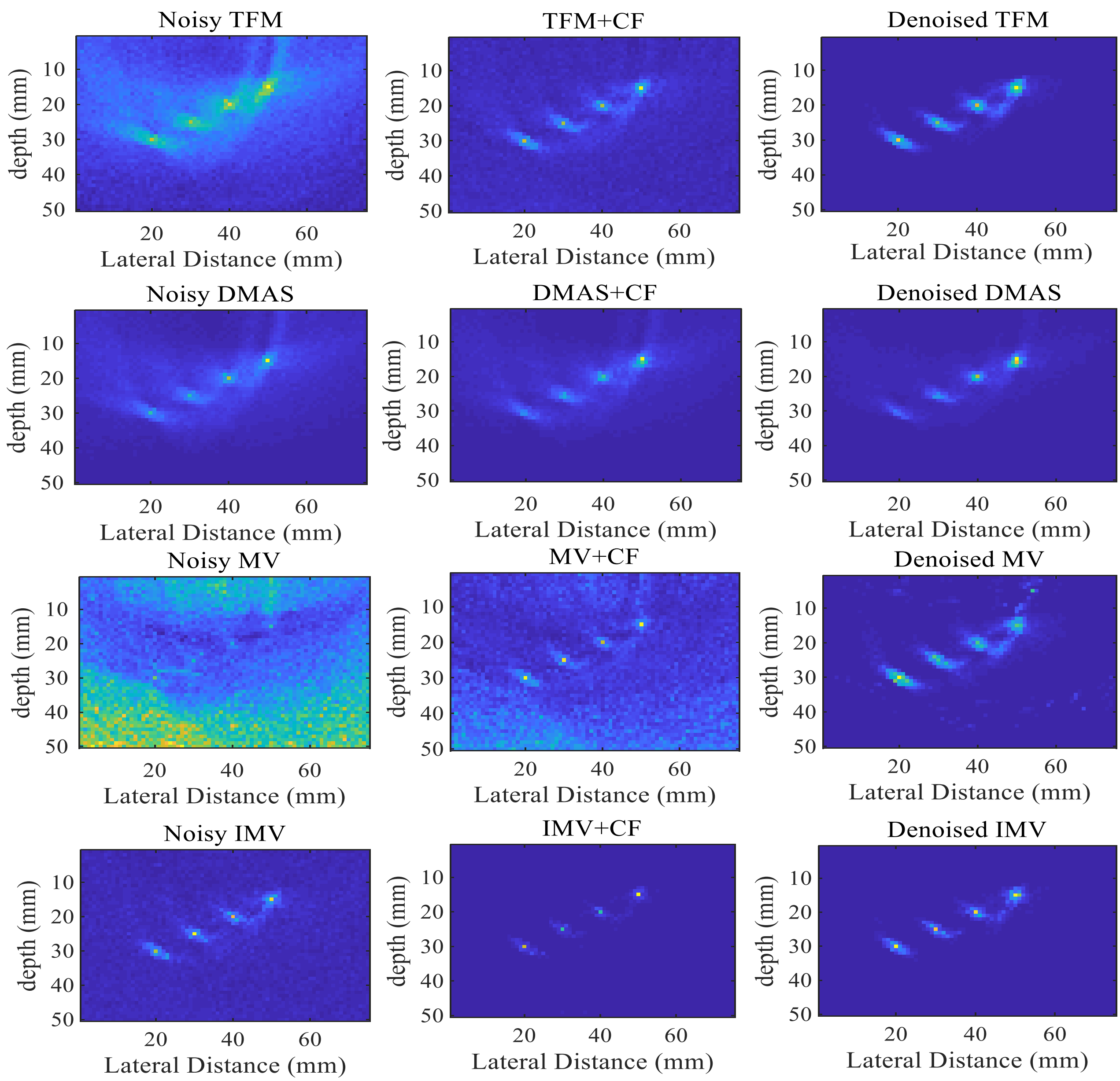

Fig. 4. Simulated images of TFM, DMAS, MV, IMV methods in three modes: Noisy mode (first column), Applying of coherence weighting alone (second column) and removal of noise by time thresholding and coherence weighting simultaneously (third column).

Fig. 7 displays the intensity plots of the proposed denoising methods. The increase in peak levels, representing the intensity of reflective points and the ability to detect defects, is well evident in the proposed methods.

It can be observed that the attenuation of peaks in this method is less than 1dB, whereas in the TFM method, this value is approximately 1.5dB, and the MV method has an attenuation of about 2dB. Additionally, with careful observation of this plot, we find that the depth of valleys between two peaks in the proposed method is lower compared to the other methods, indicating the superior ability to distinguish reflective points from each other.

Another notable point regarding the proposed denoised methods, is that background noise is reduced more than 5 dB for all of proposed beamforming methods, in comparison with their primary counterparts.

Table 2 presents the average noise level (N_{avg}), and the API metric values. It shows a reduction in API values in the proposed beamforming methods compared to the primary methods, which is considerable for TFM and MV.

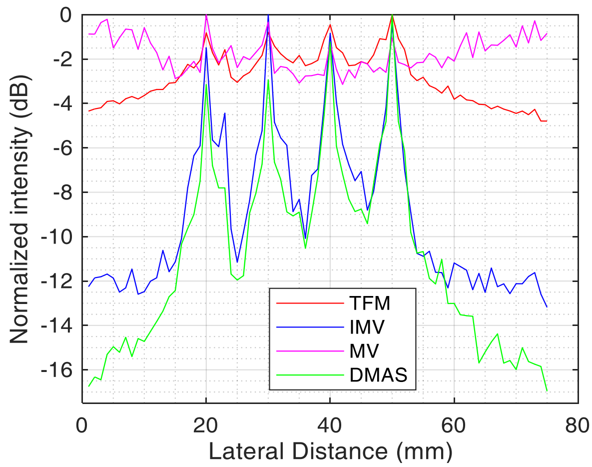

Fig. 5. Intensity function for TFM, MDAS, MV, and IMV in noisy conditions. IMV demonstrates superior noise reduction but exhibits more peak attenuation compared to the others.

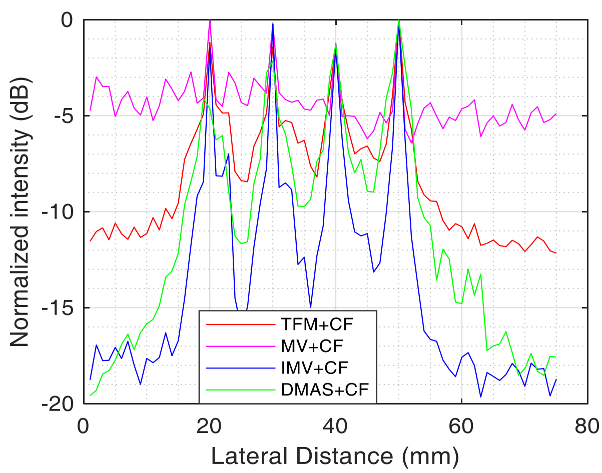

Fig. 6. Intensity function for TFM, DMAS, MV, and IMV with coherence weighting applied. IMV exhibits greater noise attenuation around the peaks, resulting in better peak distinguishing compared to the others.

Additionally, the average noise level has significantly decreased for all beamforming methods. Consequently, the proposed denoising approach has been able to demonstrate satisfactory performance in the removal of background Gaussian noise and speckle noise, while preserve the image quality of defects.

Furthermore, the performance of the proposed denoising method can be influenced by the value of p_{cf}. Table 3 shows API and N_{avg} values for four different p_{cf}. As p_{cf} increases, N_{avg} correspondingly decreases, and API slightly decreases, resulting in better resolution of reflective points. However, this improvement comes at the cost of peak attenuation, which reduces detectability for weak reflections. Moreover, computational complexity increases with higher p_{cf} values.

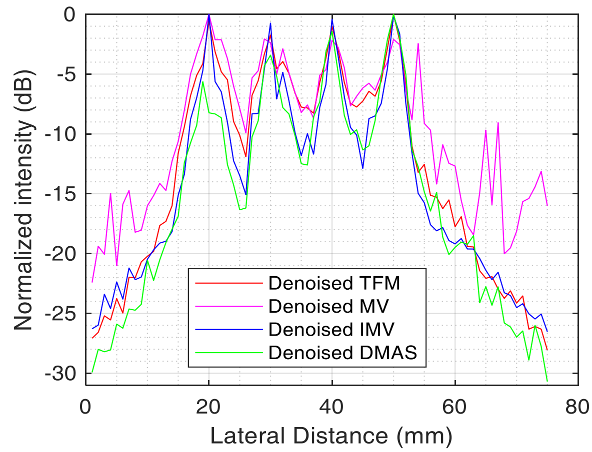

Fig. 7. Intensity function for TFM, DMAS, MV, and IMV with wavelet thresholding followed by coherence weighting. Denoised DMAS and Denoised IMV exhibit better noise attenuation than others, with Denoised IMV showing less peak attenuation compared to the others.

TABLE 2 AVERAGE BACKGROUND NOISE AND API FOR VARIOUS BEAMFORMING METHODS IN THE SIMULATION

	TFM	DMAS	MV	IMV
API	6.25	2.9	10.8	3
N_{avg}	-5.2 dB	-17.9 dB	-2 dB	-15.9 dB
	TFM+CF	DMAS+CF	MV+CF	IMV+CF
API	4.2	2.8	4.5	2.6
N_{avg}	-8.9 dB	-18.8	-7.4 dB	-19.4 dB
	Denoised TFM	Denoised DMAS	Denoised MV	Denoised IMV
API	3.8	2.8	4.8	2.9
N_{avg}	-15 dB	-23.9	-18.8 dB	-21.6 dB

TABLE 3 AVERAGE BACKGROUND NOISE AND API FOR DIFFERENT VALUES OF p_{cf} IN THE SIMULATION

p_{cf}		Denoised TFM	Denoised DMAS	Denoised MV	Denoised IMV
2	API	4.0	2.8	4.9	2.9
	N_{avg}	-12.5 dB	-23	-17.6 dB	-20.8 dB
4	API	3.8	2.8	4.8	2.9
	N_{avg}	-15 dB	-23.9	-18.8 dB	-21.6 dB
8	API	3.5	2.6	4.7	2.6
	N_{avg}	-18.6 dB	-29	-19.8 dB	-26.1 dB
12	API	3.4	2.4	4.6	2.3
	N_{avg}	-22.4 dB	-33.2	-21.1 dB	-31.2 dB

B. *Experimental results*

For the experiment, a phased array probe of model Olympus with 16 linear elements at a frequency of 7.5 MHz is used, mounted on a Rexolite wedge with the angle of 38.5 degrees[34]. The element pitch of the transducer is 0.5 mm. The width of the applied pulses is half the period of the probe, which equals 67 ns, and the amplitude of the applied pulse is 50 volts. The test piece is a cylindrical steel tube with a diameter of 60 mm and a thickness of 15 mm. The pulses received from the piece are sampled at a rate of 40 MHz. Fig. 8 shows the experimental setup.

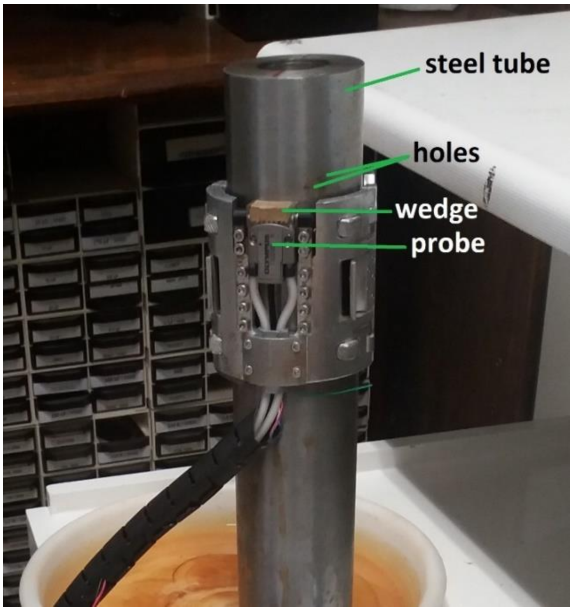

Fig. 8. The experimental setup, constructed by Niroo Research Institute (NRI) [34].

In the experiment, two small through-holes perpendicular to the axis of the steel tube at depths of 5 mm and 9 mm, each with a diameter of 0.8 mm, are provided as shown in Fig. 8. In this setup, due to the placement of the probe on the wedge, the ultrasonic waves are emitted and reflected obliquely. These waves, after passing through the wedge and entering the steel piece, are mainly transverse waves with a speed of about 3250 m/s. In this test, the lateral distance between the probe wedge and holes relative to the tube surface is 25 mm.

Figs. 9-a to 9-h show the images obtained from beamforming methods based on TFM (first row), DMAS (second row), MV (third row), and IMV (fourth row). The images in the left column show the classical methods, while the right column shows the denoised methods. The amounts of c, d, and p_{cf} are determined as before. It can be observed that in all images, the images of two holes are seen as bright spots, with their centers at depths corresponding to the locations of the holes in the steel tube. The bright areas in these images indicate background noise and speckles, which are due to the presence of noise in the signals received by the phased array and the limitations of the beamforming methods to mitigate the background noise.

It is observed that the hole images in the figures appear elongated, which is due to the significant lateral distance between the holes and the wedge compared to the length of the phased array.

According to Fig. 9, the background noise appeared in all the beamforming methods with considerable brightness, which lead to a possibility of detecting false defects, especially in the TFM and MV methods.

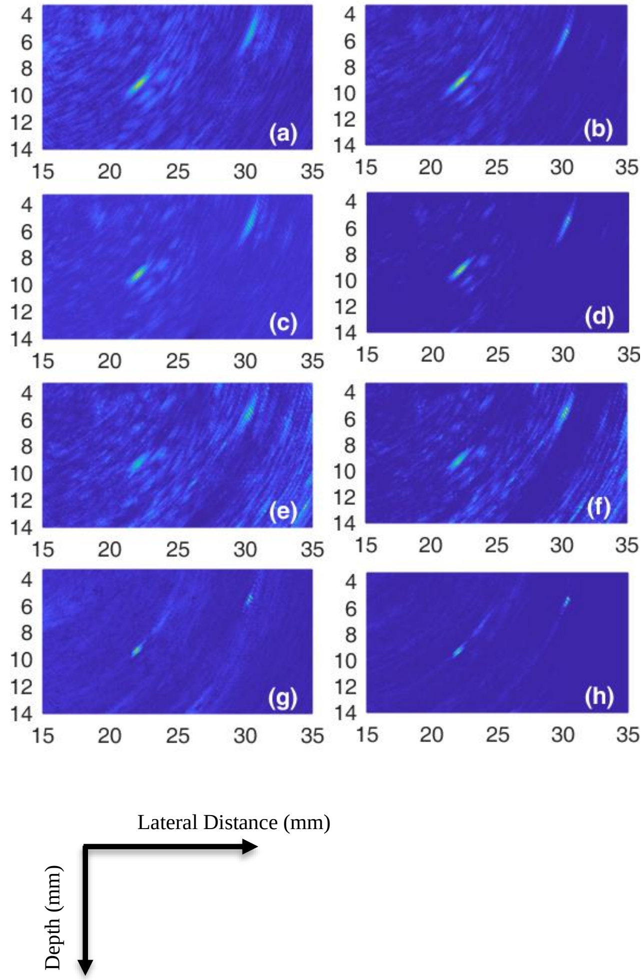

Fig. 9. The experimental images of TFM (a), Denoised TFM (b), DMAS (c), Denoised DMAS (d), MV (e), Denoised MV (f), IMV (g), Denoised IMV (h). The background noise and speckles in the proposed denoising method (the right column) are considerably less than the original images (the left column).

In the IMV and DMAS methods as shown in Fig. 9, the noise is somewhat reduced, and in IMV, the elongation of the holes reduces considerably. In the proposed denoising methods in the right column of Fig. 9, it is observed that the background noise and false reflections are significantly lower than in the counterpart methods, thereby improving the clarity of the hole images.

Table 4 presents the average background noise for the experiment. It shows a significant reduction in N_{avg} values in the proposed beamforming methods compared to the counterparts.

C. Discussion

In this study, we propose a solution to reduce background noise and speckles in phased array-based ultrasonic imaging. Our method has two main contributions: (i) denoising the phased array received signals using a novel wavelet-based thresholding technique, and (ii) applying a coherence

TABLE 4 AVERAGE BACKGROUND NOISE LEVELS FOR VARIOUS BEAMFORMING METHODS IN EXPERIMENT

	TFM	DMAS	MV	IMV
N_{avg}	-12.6 dB	-19	-10 dB	-15.4 dB
	Denoised TFM	Denoised DMAS	Denoised MV	Denoised IMV
N_{avg}	-17.4 dB	-26.6	-16.2 dB	-20.5 dB

weighting derived from the denoised signals to the output signal of the beamformer to construct the denoised images. We evaluated the proposed method on various ultrasonic beamforming techniques, including TFM, DMAS, MV, and IMV, through both simulations and experiments.

Fig. 4 qualitatively demonstrates that the combination of wavelet thresholding and coherence weighting significantly reduces background noise and speckles in beamforming techniques, while preserving the quality of reflective points. As a result, reflective points become more distinguishable in the images. The intensity functions illustrated in Figs. 5, 6, and 7 quantitatively confirm that reflective points are more discriminative after applying the proposed denoising method, consistent with the qualitative results from Fig. 4.

Additionally, the results show that DMAS and IMV provide better discrimination of reflective points and noise reduction compared to TFM and MV in both noisy and denoised versions. According to Table 2, the background noise is reduced by more than 5 dB across all beamforming methods when using the proposed denoising method, compared to their primary counterparts. Moreover, the API in the proposed denoised beamforming methods is slightly lower than in the primary counterparts, indicating improved image resolution with the proposed method.

In experiments, as shown in Fig. 9 and Table 4, the background noise is significantly lower with the proposed denoising methods than with the counterpart methods, which is consistent with the simulation results. Furthermore, Fig. 9 qualitatively shows a substantial reduction in false reflections caused by speckles in the proposed denoising methods, thereby enhancing the clarity of the holes in ultrasonic images.

V. Conclusions

In this study, we introduced a noise-robust beamforming technique aimed at reducing the speckle and background noises in ultrasonic imaging, while preserving the quality of reflective echoes. Our approach involved the utilization of a novel wavelet thresholding method on the input signals of the phase array, alongside the generation of images through total focusing method (TFM), delay-multiply-and-sum (DMAS), minimum variance (MV), and iterative MV (IMV) beamforming techniques. Subsequently, coherence weighting was derived from the denoised signals and integrated into the beamforming process to construct the denoised images. This proposed methodology not only effectively mitigates background noise but also enhances defect detection and improves the differentiation among reflective points, consequently elevating the quality and clarity of ultrasonic images.

REFERENCES

[1] J. Park, S. M. Wi, and J. S. Lee, "Computationally efficient adaptive beamformer for ultrasound imaging based on QR decomposition," *IEEE Transactions on ultrasonics, Ferroelectrics, and frequency control,* vol. 63, no. 2, pp. 256 - 265, 2016.

[2] J. Lambert, A. Pédron, G. Gens, F. Bimbard, L. Lacassagne, and E. Iakovleva, "Performance evaluation of total focusing method on GPP and GPU," *Conference on Design and Architectures for Signal and Image Processing,* pp. 1-8, 2012.

[3] L. P. Piedade, G. Painchaud-April, and P. B. A. Le Duff, "Minimum transmission events for fast ultrasonic TFM imaging: A comparative study," *NDT & E International,* vol. 128, 2022.

[4] T. Stepinski and F. Lingvall, "Synthetic aperture focusing techniques for ultrasonic imaging of solid objects," *8th European Conference on Synthetic Aperture Radar,* pp. 438-441, 2010.

[5] S. M. Sakhaei, "A decimated minimum variance beamformer applied to ultrasound imaging," *Ultrasonics,* vol. 59, pp. 119-127, 2015.

[6] A. M. Deylami and B. M. Asl, "A fast and robust beamspace adaptive beamformer for medical ultrasound imaging," *IEEE Transactions on Ultrasonics, Ferroelectrics, and Frequency Control,* vol. 64, no. 6, pp. 947-958, 2017.

[7] A. M. Deylami and B. M. Asl, " Iterative minimum variance beamformer with low complexity for medical ultrasound imaging," *Ultrasound in Medicine & Biology,* vol. 44, pp. 1882-1890, 2018.

[8] B. M. Asl and A. M. Deylami, "A low complexity minimum variance beamformer for ultrasound imaging using dominant mode rejection," *Ultrasonics, v*ol. 85, pp. 49-60, 2018.

[9] A. S. Vaidya and M. B. Srinivas, "A low-complexity and robust minimum variance beamformer for ultrasound imaging systems using beamspace dominant mode rejection," Ultrasonics, vol. 101, 2020.

[10] J. Pan, Y. Wang, Y. Wang, Z. Han, C. Zheng, and H. Peng, "Adaptive spatial smoothing-based minimum variance beamforming using signal coherence to improve image quality," IEEE International Ultrasonics Symposium (IUS), 2022.

[11] A. M. Deylami and B. M. Asl, "High resolution minimum variance beamformer with low complexity in medical ultrasound imaging," Ultrasound in Medicine & Biology, vol. 45, no. 10, pp. 2805-2818, 2019.

[12] Z. Shen, J. Li, and Q. Wu, "A fast adaptive beamformer with sidelobe control based on gradient descent ascent," Signal Processing, vol. 206, p. 108906, 2023.

[13] K. Ji, P. Zhao, C. Zhuo, H. Chen, J. Wang, and J. Fu, "High-accuracy ultrasonic imaging of the defects in the complex-surface components by the search-vector imaging condition," Mechanical Systems and Signal Processing, vol. 216, 2024.

[14] J. Wu, H. Hu, Y. Song, P. Ni, and X. Li, "Ultrasonic phased array imaging of multi-layered structures using full-matrix

migration and normalized cross-correlation matching technique," NDT & E International, vol. 145, 2024.
[15] Z. Zhao, L. Liu, W. Liu, D. Teng, Y. Xiang, and F. Z. Xuan, "Discretized tensor-based model of total focusing method: A sparse regularization approach for enhanced ultrasonic phased array imaging," NDT & E International, vol. 141, 2024.
[16] D. Teng, L. Liu, Y. Xiang, and F. Z. Xuan, "An optimized total focusing method based on delay-multiply-and-sum for nondestructive testing," Ultrasonics, vol. 128, 2023.
[17] N. Molinier, G. Painchaud-April, A. L. Duff, M. Toews, and P. Bélanger, "Ultrasonic imaging using conditional generative adversarial networks," Ultrasonics, vol. 133, 2023.
[18] H. Yang, J. Shu, S. Li, and Y. Duan, "Ultrasonic array tomography-oriented subsurface crack recognition and cross-section image reconstruction of reinforced concrete structure using deep neural networks," Journal of Building Engineering, vol. 82, 2024.
[19] G. Granados, R. Miorelli, F. Gatti, S. Robert, and D. Clouteau, "Towards a multi-fidelity deep learning framework for a fast and realistic generation of ultrasonic multi-modal Total Focusing Method images in complex geometries," NDT & E International, vol. 139, 2023.
[20] A. Ghaedi, R. Sedaghati, M. Mahmoudian, and S. Bazyari, "De-noising of partial discharge signals in HV XLPE cables by reference noise based on the wavelet transform," International Journal of Industrial Electronics Control and Optimization, vol. 6, no. 4, pp. 291-306, 2023.
[21] A. M. Deylami and B. M. Asl, "Improving the coherence coefficient resistance in ultrasonic beamforming," Twenty-Third Iranian Conference of Electrical Engineering, Sharif University of Technology, May 2015.
[22] J. Lester and W. Schmmer, "Fundamentals of ultrasonic phased arrays," Springer, 2014.
[23] M. Bekrani and V. Hamiyati-Vaghef, "An improved method for ultrasound imaging in weld inspection," Iranian Journal of Electrical and Electronic Engineering, vol. 17, no. 1, pp. 45-59, 2020.
[24] M. Bekrani, "Phased array ultrasonic imaging using improved total focusing method based on beamforming in non-destructive test," Journal of Welding Science and Technology of Iran, vol. 6, no. 1, pp. 115-132, 2020.
[25] B. Widrow and S. D. Stearns, "Adaptive signal processing," Prentice-Hall,1985.
[26] G. O. Y. M . Misiti, and J. M. Poggi, "Wavelets and their applications," John Wiley & Sons, 2013.
[27] F. Ping and L. Xinbao, "An improved denoising method for ultrasonic echo of non-destructive evaluation," IEEE International Conference on Anti-counterfeiting, Security, and Identification (ASID), 2016.
[28] R. S. V. Matz, S. Starman, and M. Kreidl, "Signal-to-noise ratio enhancement based on wavelet filtering in ultrasonic testing," Ultrasonics, vol. 49, pp. 752-759, 2009.
[29] D. L. Donoho, "De-noising by soft-thresholding," IEEE Transactions on Information Theory, vol. 41, no. 3, pp. 613-627, 1995.
[30] T. F. Sanam and C. Shahnaz, "Noisy speech enhancement based on an adaptive threshold and a modified hard thresholding function in wavelet packet domain," Digital Signal Processing, vol. 23, pp. 941-951, 2013.
[31] J. Camacho, M. Parrilla, and C. Fritsch, "Phase coherence imaging," IEEE Transactions on Ultrasonics, Ferroelectrics, and Frequency Control, vol. 56, no. 5, pp. 958-974, 2009.
[32] B. K. G. R. Baiotto, C. Nageswaran, and T. Clarke, " "Coherence weighting applied to FMC/TFM data from austenitic CRA clad lined pipes," Journal of Nondestructive Evaluation, vol. 37, no. 49, 2018.
[33] B. W. D. C. Holmes and P. D. Wilcox, "Post-processing of the full matrix of ultrasonic transmit–receive array data for non-destructive evaluation," NDT & E International, vol. 38, pp. 701-711, 2005.
[34] M. Bekrani and V. Hamiyati-Vaghef, "A new method for designing and implementation of NDT weld inspection of boiler tubes using ultrasonic phased array," Electronics Industries, vol. 12, no. 4, pp. 39-51, 2022.

Mozhgan Ehsani was born in Tehran, Iran. She received her Bachelor's degree in Electrical and Electronics Engineering in 2015 and her Master's degree from Qom University of Technology, Qom, Iran, in 2023. From 2019 to 2020, she worked as a designer at Matin Electronic Company. Her research has focused on ultrasound waves, with current interests in the development of ultrasonic beamformers.

Mehdi Bekrani received his B.Sc. degree in Electrical Engineering from Ferdowsi University of Mashhad, Iran, in 2002, and earned his M.Sc. and Ph.D. degrees in Electrical Engineering from Tarbiat Modares University, Tehran, Iran, in 2004 and 2010, respectively. From 2010 to 2012, he was a Research Fellow at Nanyang Technological University, Singapore. He then joined the Department of Electrical and Computer Engineering at Qom University of Technology, Qom, Iran, as an Assistant Professor and currently serves as an Associate Professor. His research interests focus on adaptive signal processing and its applications.

Solyman Garousi was born in Tehran, Iran, in 1991. He earned his Bachelor's degree in Electronics Engineering from Islamic Azad University, Karaj Branch, Alborz, Iran, in 2016, and his Master's degree in Electronics Engineering from Qom University of Technology in 2019. Since 2019, he has been a researcher at the Iran Electronics Technology Institute in Tehran, Iran. His research interests include audio and ultrasonic signal processing, navigation and communication signal processing, and image processing.